

See discussions, stats, and author profiles for this publication at: <https://www.researchgate.net/publication/231647265>

# Shape-Controlled Synthesis of Silver and Palladium Nanoparticles Using $\beta$ -Cyclodextrin

ARTICLE in THE JOURNAL OF PHYSICAL CHEMISTRY C · JUNE 2011

Impact Factor: 4.77 · DOI: 10.1021/jp200662j

CITATIONS

30

READS

88

## 4 AUTHORS:



**Hafedh Kochkar**

University of Tunis El Manar

59 PUBLICATIONS 523 CITATIONS

SEE PROFILE



**Aouine Mimoun**

Claude Bernard University Lyon 1

64 PUBLICATIONS 727 CITATIONS

SEE PROFILE



**A. Ghorbel**

Faculté des Sciences de Tunis

260 PUBLICATIONS 1,618 CITATIONS

SEE PROFILE



**Gilles Berhault**

French National Centre for Scientific Research

133 PUBLICATIONS 1,758 CITATIONS

SEE PROFILE


# Shape-Controlled Synthesis of Silver and Palladium Nanoparticles Using $\beta$ -Cyclodextrin

Hafedh Kochkar,<sup>\*,†</sup> Mimoun Aouine,<sup>‡</sup> Abdelhamid Ghorbel,<sup>§</sup> and Gilles Berhault<sup>\*,‡</sup>

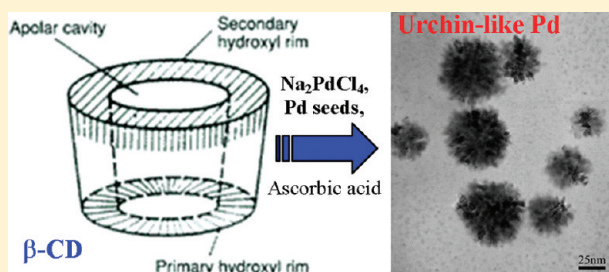
<sup>†</sup>Centre National de Recherches en Sciences des Matériaux (Cnrs), Technopôle de Borj-Cédria, 2050, Hammam-Lif, Tunisia

<sup>‡</sup>Institut de Recherches sur la Catalyse et l'Environnement de Lyon, Umr 5256 CNRS-Université de Lyon, 2 avenue Albert Einstein, 69100 Villeurbanne, France

<sup>§</sup>Laboratoire de Chimie des Matériaux et Catalyse, Faculté des Sciences de Tunis, 2092, Tunisia

 Supporting Information

**ABSTRACT:** Shape-controlled silver and palladium nanoparticles were for the first time synthesized by seed-mediated techniques in the presence of  $\beta$ -cyclodextrin ( $\beta$ -CD). Palladium and silver seeds were prepared by reduction of palladium or silver ions with sodium borohydride in the presence of sodium citrate dihydrate as a stabilizer. Seeds were then injected into a “growth” solution containing the same Pd (or Ag) precursor, ascorbic acid (as a weak reducing agent), and  $\beta$ -CD. Using  $\beta$ -cyclodextrin impacts the final morphology of silver nanoparticles through a strong capping effect slowing down the growth regime and shifting it to thermodynamic-controlled conditions. Adjusting the  $\beta$ -CD/Ag molar ratio can lead to the selective formation of multiply twinned icosahedral particles presenting mainly  $\{111\}$  facets. On palladium,  $\beta$ -cyclodextrin selectively led to the controlled aggregation of primary nanoparticles into nanodendrites or multipods. After deposition on  $\text{TiO}_2$ , these nanostructured Pd catalysts show excellent activity for the hydrogenation of cinnamaldehyde.



## 1. INTRODUCTION

Colloidal techniques to synthesize shape-controlled metallic nanoparticles (NPs) have been tremendously developed in the last 10 years due to a great interest in materials science for the unusual optical properties of anisotropic nanocrystals.<sup>1–5</sup> Indeed, rods, wires, and nanoplates present plasmonic properties which depend on their morphology.<sup>6</sup> Anisotropic Ag and Au particles can also exhibit coupling of their plasmon bands with adsorbed molecules' electronic states, leading to a huge increase in the detection limit of these adsorbates, i.e., the so-called Surface-Enhanced Raman Scattering (SERS) effect.<sup>7</sup> These nanostructured particles are therefore good candidates as chemical and biological sensors.<sup>8</sup>

The synthesis of shape-controlled metallic nanoparticles has also recently opened the way to new applications in catalysis.<sup>9–20</sup> Control of the shape of a metallic nanocrystal leads to well-defined morphologies characterized by the preferential exposition of crystallographic planes. This selective exposition of facets allows us to establish direct surface structure–reactivity relationships for structure-sensitive reactions contrary to isotropic particles presenting a high proportion of defects, corners, or edge sites with high index facets.<sup>14,17,19,20</sup> The preparation of shape-controlled noble metallic (Pd, Pt, Rh) nanoparticles has led to catalytic systems with high potentialities particularly for selectivity issues.<sup>9,13,14,17,19,20</sup> Berhault et al.<sup>13</sup> found that an increasing proportion of  $\{111\}$  facets on shape-defined Pd NPs supported

on  $\alpha\text{-Al}_2\text{O}_3$  led to a higher selectivity to butenes for the hydrogenation of 1,3-butadiene. Lee et al.<sup>19</sup> observed that tetrahedral Pt particles with  $\{111\}$  facets promote the selective promotion of the trans-to-cis isomerization of olefins. Bratlie et al.<sup>14</sup> have observed that cubic Pt particles with  $\{100\}$  facets only led to cyclohexane selectivity during the hydrogenation of benzene.

The shape-controlled formation of metallic nanocrystals can be monitored through the selective adsorption of surfactants, ligands, or polymers on specific crystallographic facets leading to a preferential growth along another (or other) direction(s). Two different strategies are generally employed in colloidal techniques: the polyol process using a polymer, generally poly(vinylpyrrolidone) (PVP), in organic solvents<sup>21</sup> or the aqueous-mediated use of surfactants, generally alkyltrimethylammonium halides.<sup>22</sup>

The morphological control of metallic NPs has largely progressed over recent years leading to a fine shape tuning of their nanostructure. The range of available morphologies has been considerably extended to octahedral,<sup>23–28</sup> icosahedral,<sup>24,29–33</sup> bipyramidal,<sup>34,35</sup> or multipod-like.<sup>36–39</sup> This fine-tuning of the NP morphology is however partially accompanied by progress in

**Received:** January 21, 2011

**Revised:** April 4, 2011

**Published:** May 20, 2011

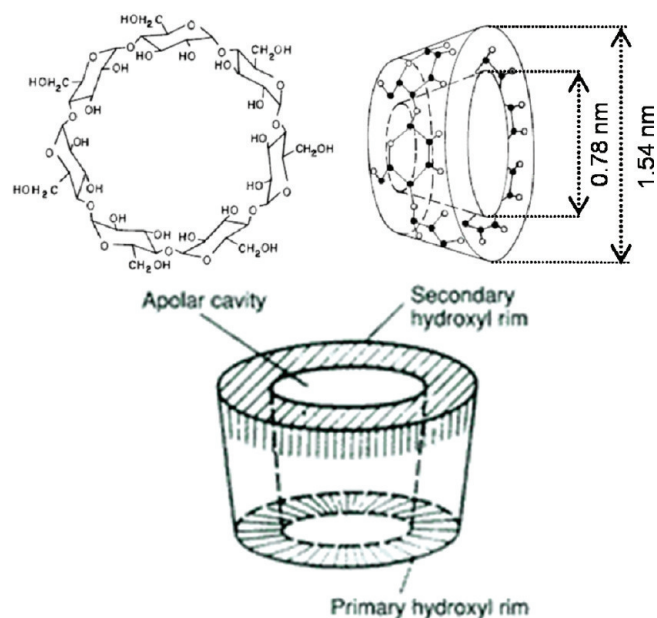


**Figure 1.** Structure of  $\beta$ -CD and schematic representations of hydrophobic (primary rim) and hydrophilic (secondary rim) regions.

understanding the growth mechanism leading to the selective formation of a particular shape. This situation results from the interference of multiple parameters influencing the growth regime and the final morphology. The main parameters are the seed structure<sup>40–43</sup> but also several parameters influencing the kinetic or thermodynamic growth regime like the seed concentration,<sup>44–46</sup> the nature of the capping agents,<sup>47–50</sup> and the nature and concentration of reducing agents,<sup>51</sup> or the concentration of metallic precursor.<sup>52</sup> Moreover, the classical crystallization theory describing growth by molecule or ion-by-ion attachment cannot be solely considered. For example, for Pd nanocrystals formed by the seed-mediated technique, oriented attachment of primary nanoparticles onto seeds predominantly occurred during the early growth process.<sup>53</sup>

Another important issue for improving colloidal techniques for the preparation of metallic nanocrystals is to develop “greener” synthesis approaches. The use of an aqueous media for the surfactant-directed growth technique is in accordance with the principles of green chemistry. This is also true for the reducing agent: ascorbic acid (vitamin C). A further step to a greener process will be the replacement of alkyltrimethylammonium halides by biocompatible agents. In this respect, cyclodextrins (CDs), soluble nontoxic molecules, have been increasingly used for the preparation of metallic nanoparticles such as gold,<sup>54–57</sup> silver,<sup>58</sup> palladium,<sup>59</sup> and platinum.<sup>60</sup>

CDs are a group of cyclic oligosaccharides composed of six ( $\alpha$ -CD), seven ( $\beta$ -CD), or eight ( $\gamma$ -CD)  $\alpha$ (1,4)-linked glucopyranose units. The oligosaccharides form a truncated cone with primary OH groups directed to the narrow side (primary face), and secondary OH groups are on the wide side of the torus (secondary face) (Figure 1) leading for example to cavities of 7.8 Å for  $\beta$ -CD. While the –OH groups on both faces are capable of intramolecular H-bonding, the H-bonds may be disrupted by distortion of the glucopyranose units. As a result, more extensive H-bonds are formed on the primary rim due to the flexibility of primary OH groups compared to the secondary OH groups on the second rim, rendering CDs amphipathic.<sup>61</sup> While the primary

face presents hydrophobic character, the secondary face remains hydrophilic. Up to now, the use of cyclodextrins for synthesizing shape-controlled metallic nanocrystals was only envisaged for Au nanoparticles.<sup>54–57</sup> Apart from non-well-defined nanochains,<sup>54</sup> the synthesis strategy was generally based on the combined use of  $\beta$ -CD with surfactants (dodecyltrimethylammonium bromide (DTAB)<sup>57</sup> or *N*-dodecyl-*N,N*-dimethyl-3-ammonio-1-propanesulfonate<sup>56</sup>) leading to dendritic morphologies with very large sizes (from 200 nm up to several micrometers). The potential usefulness of cyclodextrins as a greener alternative to alkyltrimethylammonium halides for synthesizing metallic nanocrystals was therefore determined in the present study for the two important Ag and Pd catalytic systems.

We used here the seed-mediated growth approach to make nanostructured Ag and Pd in aqueous solution. In this paper, we used 3–6 nm Ag or Pd isotropic particles (seeds) to prepare nanostructured silver and palladium. The silver seeds were prepared by reduction of silver nitrate with sodium borohydride in the presence of citrate as stabilizer. Careful control of the growth conditions was monitored using a weak reducing agent (ascorbic acid) and  $\beta$ -CD (seven glucose units) in aqueous solution. Temperature and pH were kept constant.  $\beta$ -CD/metal molar ratios were varied from 20 to 300. Pd and Ag showed different interactions with  $\beta$ -CD molecules. While silver multiply twinned icosahedral particles were obtained at high  $\beta$ -CD/Ag ratio, multibranching palladium nanoparticles with nanodendritic shape were selectively formed. Finally, after deposition onto  $\text{TiO}_2$ , the Pd catalysts were tested for the selective hydrogenation of cinnamaldehyde to evaluate the catalytic properties of the as-formed Pd nanoparticles obtained for different  $\beta$ -CD/Pd ratios.

## 2. EXPERIMENTAL METHODS

**2.1. Materials.** Silver nitrate ( $\text{AgNO}_3$ , 99.99%), sodium tetrachloropalladate ( $\text{Na}_2\text{PdCl}_4$ , 99.9%), sodium citrate dihydrate ( $\text{Na}_3\text{C}_6\text{H}_5\text{O}_7 \cdot 2\text{H}_2\text{O}$ , 99%), sodium borohydride ( $\text{NaBH}_4$ , 99%), ascorbic acid ( $\text{C}_6\text{H}_8\text{O}_6$ , 99%), and  $\beta$ -cyclodextrin ( $\beta$ -CD 99%) were purchased from Aldrich. Sodium hydroxide ( $\text{NaOH}$ , Fisher Chemicals) and hydrochloric acid ( $\text{HCl}$ , Panreac Quimica) were used without further purification. For the preparation of all samples, ultra pure water ( $18 \text{ M}\Omega \cdot \text{cm}^{-1}$ ) was used throughout the whole experiment.

**2.2. Preparation of Silver Seeds.** A 10 mL aqueous solution containing 0.25 mM  $\text{AgNO}_3$  and 0.25 mM sodium citrate dihydrate was prepared. Next, 25  $\mu\text{L}$  of ice-cold 0.1 M freshly prepared  $\text{NaBH}_4$  solution was quickly injected into the solution while stirring vigorously. The color of the solution was immediately changed to light yellow. The average particle size was found to be around 5 nm. In this step, sodium citrate dihydrate serves only as a stabilizer since it cannot reduce the silver salt at room temperature.<sup>62</sup>

**2.3. Preparation of Palladium Seeds.** A 10 mL aqueous solution containing 0.25 mM  $\text{Na}_2\text{PdCl}_4$  and 0.25 mM sodium citrate dihydrate was prepared. Next, 25  $\mu\text{L}$  of ice-cold 0.1 M freshly prepared  $\text{NaBH}_4$  solution was injected into the solution all at once while stirring vigorously. The color of the solution was immediately changed to black.

**2.4. Preparation of Silver Growth Solutions.** A 50 mL aqueous solution containing 0.005 M  $\beta$ -CD was prepared. Next, a variable amount of 0.025 M  $\text{AgNO}_3$  was added to monitor the  $\beta$ -CD/Ag molar ratio from 50 to 150 (50, 80, and 150). As an example, using the  $\beta$ -CD/Ag = 50, the following recipe was used:



to 50 mL of 0.005 M  $\beta$ -CD solution, 200  $\mu$ L of  $\text{AgNO}_3$  (0.025 M) and 1.0 mL of freshly prepared ascorbic acid (0.1 M) were added. Silver seed solution (100  $\mu$ L) was then injected. Finally, 500  $\mu$ L of 0.1 M NaOH was added to reach neutral pH. The molar ratio between Ag in the seed solution and Ag in the growth solution was kept constant at  $5 \times 10^{-3}$ . Within 2–3 min, the solution color changed into yellow-greenish gray as a function of  $\beta$ -CD/Ag molar ratios. The growth solutions were left undisturbed for 24 h before TEM analysis.

**2.5. Preparation of Palladium Growth Solutions.** A 50 mL aqueous solution containing 0.005 M  $\beta$ -CD was prepared. Next, a variable amount of 0.005 M  $\text{Na}_2\text{PdCl}_4$  was added to monitor the  $\beta$ -CD/Pd molar ratio from 20 to 150 (20, 50, 100, and 150). Freshly prepared ascorbic acid (1.0 mL, 0.1 M) was added. Finally, 100  $\mu$ L of palladium seed solution was injected. A variable amount of 0.1 M NaOH was added to reach neutral pH. The growth solutions were left undisturbed for 24 h before TEM analysis.

**2.6. Sample Characterization.** Transmission electron microscopy studies were performed using a JEOL JEM 2010 operating at 200 kV and equipped with EDS capabilities. The microscope is equipped with an ultrahigh resolution polar piece (point resolution: 1.9 Å). Specimens for the TEM studies were prepared by depositing a drop of aqueous suspension of the samples onto a 300 mesh Cu grid, coated with a lacey carbon film and leaving the grid to dry. The samples were stable under the electron beam and did not degrade within the typical observation times. Particle size distributions and corresponding statistical analysis of the different morphological types of nanoparticles were obtained from TEM images by using analySIS software to record digital images, while the SigmaScan Pro 5.0 program was used for particle morphology measurements and statistical counting. To determine the proportion of Ag or Pd involved in each type of nanoobject, yields of Ag or Pd per nanoobjects were calculated taking into account their respective volumes.<sup>31</sup> This yield (or volumic percentage) was calculated according to the following equation

$$Y_j (\%) = \frac{\sum_i n_i v_i}{\sum_{j=1}^n \sum_i n_i v_i} \quad (1)$$

with  $n_i$  being the number of particles of a given volume  $v_i$ , and  $j = 1, \dots, n$  being a given type of nanoobject (cubes, rods, tetrahedron, ...). This yield per nanoobject or volumic percentage provides useful complementary information besides the statistical distribution.

**2.7. Catalytic Evaluation of Pd NPs in the Selective Hydrogenation of Cinnamaldehyde.** The Pd nanoparticles were first deposited onto  $\text{TiO}_2$  (Degussa P25,  $S_{\text{BET}} = 40 \text{ m}^2/\text{g}$ ). The role of the  $\text{TiO}_2$  support was to provide stabilization of the Pd NPs avoiding their aggregation during the course of the reaction. The Pd NPs after their synthesis in aqueous solution according to the procedure described in Section 2.5 were centrifuged at 3000 rpm for 45 min to reduce the volume from 200 to 2 mL. This concentrated solution was impregnated onto  $\text{TiO}_2$ . After maturation for 24 h at 303 K, the solid was washed with ethanol to remove  $\beta$ -CD and dried for 48 h at 303 K. Catalysts are labeled Pd(X)/ $\text{TiO}_2$  with X being the  $\beta$ -CD/Pd molar ratio used to prepare the Pd NPs. Pd loading (determined by ICP-AES) was around 0.2 wt %. For comparison purposes, a reference isotropic Pd/ $\text{TiO}_2$  catalyst was also synthesized by simple impregnation of

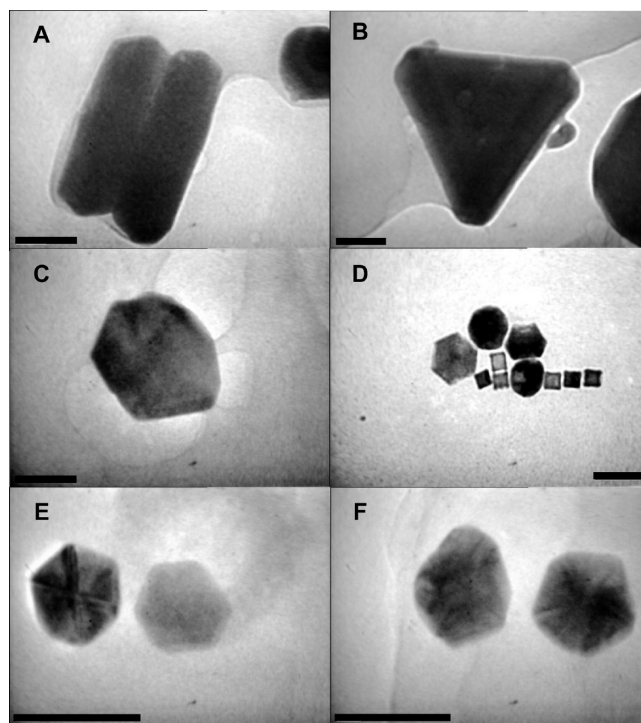


**Figure 2.** TEM images of the different types of nanocrystals obtained at a  $\beta$ -CD/Ag molar ratio of 50 (A–C) (A, nanorods; B, triangular nanoplate; C, icosahedron), 80 (D) (icosahedra and cubes), and 150 (E–F) (icosahedra and a few decahedra). Scale bars: 100 nm.

$\text{Na}_2\text{PdCl}_4$  onto  $\text{TiO}_2$  P25. The as-impregnated solid was then contacted with  $\text{NaBH}_4$  in excess to reduce Pd. The reduced catalyst was then thoroughly washed with water and ethanol before being dried for 48 h at 303 K. The final Pd loading was 0.40 wt %.

Cinnamaldehyde hydrogenation was then performed in the liquid phase using a laboratory scale stainless-steel Parr 4560 batch reactor working under static conditions. The batch was first filled with 150 mL of isopropanol. About 80 mg of the Pd/ $\text{TiO}_2$  catalyst was then put into contact with 400 mg of cinnamaldehyde at room temperature under 10 bar of nitrogen. The autoclave was then purged three times with  $\text{N}_2$  before being heated at 323 K. When the final temperature was reached, the autoclave was finally pressurized under 10 bar  $\text{H}_2$  and then stirred at 500 rpm. The course of the reaction was followed by analyzing samples using gas chromatography (VARIAN CP 3380—plot alumina column PONA,  $L = 50 \text{ m}$ , split injector; FID detection) at regular time intervals considering the beginning of the stirring as the initial reaction time. No detectable Pd leaching was observed during the catalytic test.

### 3. RESULTS AND DISCUSSION

**3.1. Formation of Shape-Controlled Ag Nanoparticles.** The use of  $\beta$ -cyclodextrin ( $\beta$ -CD) as a shape-controlling agent for synthesizing well-defined nanoparticles was first investigated in the case of silver. Figures 2 and S1 (Supporting Information) report the different types of morphologies obtained at three different molar  $\beta$ -CD/Ag ratios (50, 80, 150), keeping the Ag precursor concentration constant.  $\beta$ -CD strongly influences the relative proportions of Ag nanoobjects which can be synthesized

**Table 1.** Statistical Frequency (%) and Yield (%) (or Volumic Percentage) of the Different Types of Silver Nanocrystals Synthesized at  $\beta$ -CD/Ag Molar Ratios of 50, 80, and 150<sup>a</sup>

$\beta$ -CD/Ag molar ratio	50	80	150
icosahedra	33 (59)	53 (83)	85 (90)
rods	23 (18)	5 (9)	9 (8)
cubes	/	38 (7)	3 (1)
bipyramids	6 (7)	/	/
triangular nanoplates	25 (7)	4 (1)	3 (1)
disk-like	13 (9)	/	/

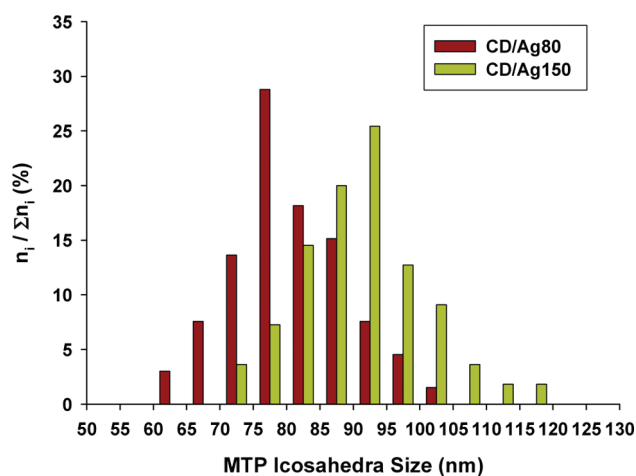
<sup>a</sup>Yield values are given in parentheses.**Table 2.** Dimensions in Nanometers of the Different Types of Silver Nanocrystals Formed at  $\beta$ -CD/Ag Molar Ratios of 50, 80, and 150

$\beta$ -CD/Ag molar ratio	50	80	150
icosahedra	215 $\pm$ 43	171 $\pm$ 37 <sup>a</sup> 79 $\pm$ 8 <sup>a</sup>	92 $\pm$ 8
rods	$L = 291 \pm 30$ $D = 106 \pm 20$ $AR^b = 2.9 \pm 0.7$	$L = 135 \pm 55$ $D = 78 \pm 22$ $AR^b = 1.7 \pm 0.2$	$L = 110 \pm 11$ $D = 64 \pm 5$ $AR^b = 1.7 \pm 0.3$
cubes	/	40 $\pm$ 11	69 $\pm$ 9
bipyramids	205 $\pm$ 30	/	/
triangular nanoplates	223 $\pm$ 27	111 $\pm$ 22	102 $\pm$ 3
disk-like	272 $\pm$ 29	/	/

<sup>a</sup>The size distribution of silver icosahedra at a  $\beta$ -CD/Ag molar ratio of 80 presents a bimodal evolution. <sup>b</sup>AR is the aspect ratio ( $L/D$  of each particle).

using a citrate-capped seed-mediated technique (Table 1). At a  $\beta$ -CD/Ag molar ratio of 50, a mixture of different morphologies was achieved comprising multiply twinned icosahedra (33%), 5-fold twinned nanorods (23%), and triangular nanoplates (25%). Disk-like nanoplates (13%) and bipyramids were also produced to a lower extent. Increasing the  $\beta$ -CD/Ag molar ratio to 80 led to a higher proportion of multiply twinned icosahedral particles (53%) and to the formation of cubic particles. All other morphologies decreased in proportion (nanorods, triangular nanoplates) or even disappeared (bipyramids, disk-like nanoplates). A further increase in the  $\beta$ -CD concentration leading to a  $\beta$ -CD/Ag molar ratio of 150 results in the selective formation of icosahedral NPs (85%) with low percentages of secondary products (nanorods, cubes, and triangular nanoplates). Using yield values per nanoobject, the proportion of Ag used to synthesize icosahedral particles is even higher (due to their relatively bigger size) reaching up to 90% for the  $\beta$ -CD/Ag molar ratio of 150 (Table 1). Yield values for other nanoobjects never reach percentages higher than 10% except for the Ag nanorods at a  $\beta$ -CD/Ag molar ratio of 50. The high statistical proportion of cubes (38%) at a  $\beta$ -CD/Ag molar ratio of 80 corresponds only to a low yield value of 7% due to the relatively smaller average size of this type of silver nanocrystal.

Increasing the  $\beta$ -CD concentration generally led to a strong decrease of the particle size particularly in the  $\beta$ -CD/Ag molar ratio range 50–80 (Table 2). The further increase of this ratio up to 150 led to a less marked decrease in size (Table 2). This effect is particularly emphasized for the 5-fold twinned Ag nanorods with a decrease of both dimensions (length and width) with the

**Figure 3.** Size distributions of icosahedra particles obtained at  $\beta$ -CD/Ag ratios of 80 and 150. For clarity purposes, at  $\beta$ -CD/Ag = 80, only the first distribution centered at 78 nm is shown (see text).

increasing concentration of  $\beta$ -CD. Since 5-fold twinned Ag nanorods are formed of {111} extremities and lateral {100} facets,<sup>63</sup>  $\beta$ -CD seems to restrain particle growth in both directions by interacting with both (100) and (111) Ag planes. However, since the aspect ratio AR ( $AR = \text{length}/\text{width}$ ) decreases when increasing the  $\beta$ -CD/Ag molar ratio from 50 to 80,  $\beta$ -CD would interact more strongly with (111) planes leading to a less restrained transversal growth. For the particular case of multiply twinned icosahedra, the decrease in particle size with increasing  $\beta$ -CD concentration is in fact accompanied by the formation of two distinct populations at the  $\beta$ -CD/Ag molar ratio of 80 (Table 2). While the most important population (78%) is still formed of particles with a relatively bigger size ( $171 \pm 37$  nm), the second population is formed of smaller NPs ( $79 \pm 8$  nm). The size of the bigger particles still tends to decrease with the increasing concentration of  $\beta$ -CD, confirming a growth restraining effect of the oligosaccharide molecule. At the  $\beta$ -CD/Ag molar ratio of 150, the asymmetric size distribution (Figure 3) (with higher proportions on the lower side of the histogram) suggests an overlap of the two distinct populations with still a decrease in size of the former bigger population observed previously at the  $\beta$ -CD/Ag molar ratio of 80, while the smaller size distribution would hardly change in size. This bimodal distribution at  $\beta$ -CD/Ag = 80 suggests a nonhomogeneous interaction of  $\beta$ -CD with citrate-capped growing seeds at this intermediate oligosaccharide concentration.

The morphology of metallic nanocrystals obtained using seed-mediated techniques depends on several experimental parameters (concentrations and nature of capping<sup>47–50</sup> and reducing agents,<sup>51</sup> amount of seeds injected into the growth solution,<sup>44–46</sup> concentration of metallic precursor<sup>52</sup>) which could influence the growth regime shifting it from a kinetically to a thermodynamically controlled growth. While equilibrium nanocrystals with a “rounded” aspect and low energy facets will be formed under a thermodynamic growth regime, anisotropic nanocrystals with higher surface areas and metastable high energy facets will be favored under a kinetic regime.<sup>64</sup> In the present study, only the  $\beta$ -CD concentration is varied, while the concentrations in  $\text{AgNO}_3$ , citrate (for the seed solution), and ascorbic acid are similar for all the different growth solutions. The progressive shift from a partially kinetically controlled growth (with 38% of 2D nanoplates)

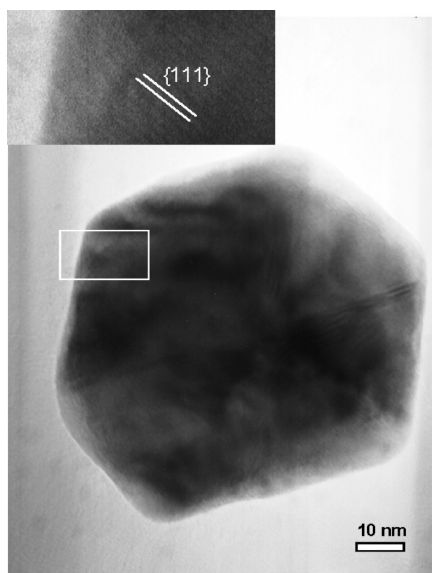


**Figure 4.** TEM image of an icosahedral Ag nanocrystal obtained at a  $\beta$ -CD/Ag molar ratio of 150. Twinning planes can be seen running from the edge to the center of the particle. Inset: enlarged image of the white square region showing the presence of  $\{111\}$  fringes.

to a thermodynamically controlled one (favoring the selective formation of multiply twinned icosahedra) cannot be ascribed to any reducing effect increasing with the concentration of  $\beta$ -CD used in the growth solution. Indeed,  $\beta$ -CD would play a reducing role but only under basic conditions (pH = 10–12).<sup>55</sup> In the experimental conditions used here, the growth solution was stabilized at pH = 7 rejecting any possible reducing effect due to the  $\beta$ -CD molecule.

The morphology of nanocrystals will also depend on the stabilized structure of the seed on which the addition of monomers will occur.<sup>40–43,65</sup> Seeds are formed through reduction of the  $\text{AgNO}_3$  precursor to form zerovalent Ag atoms which aggregate to form nuclei. These nuclei will have relatively stable crystallinity and well-defined facets after reaching a critical size. During their growth in solution, twin defects can be formed in the seed leading to an extra strain energy which can be compensated by increasing the proportion of the low surface energy  $\{111\}$  facets.<sup>66</sup> Single-crystalline, single-twinned, and multiply twinned (both decahedral and icosahedral) structures can then be obtained, and their respective proportions will strongly depend on the size of the seeds. If the multiply twinned seeds grow too rapidly, the extra strain energy due to the twin defects cannot be compensated anymore by the formation of low surface energy  $\{111\}$  facets leading to their evolution into single-twinned seeds or single-crystalline cubooctahedra.<sup>67</sup> Growth must then be slowed down to allow the formation of multiply twinned seeds evolving into either icosahedral particles or 5-fold-twinned nanorods (if starting from decahedral particles). According to the respective proportions of nanoobjects obtained when increasing the  $\beta$ -CD concentration, results suggest that  $\beta$ -CD will help to restrain the growth of the seeds leading to a longer time for seeds at smaller sizes. This favors the formation of icosahedral multiply twinned particles (MTPs). In this respect, the HRTEM picture of an icosahedral Ag particle (Figure 4) confirms the formation of a hexagonal morphology (partly deformed when  $\beta$ -CD is present) presenting twinning planes running from the

edge to the center of the particle. An enlarged image of one of the sets of planes (inset Figure 4) reveals the presence of fringes corresponding to the  $d$  spacing of 2.35 Å of Ag(111) planes.

At a  $\beta$ -CD/Ag molar ratio of 50,  $\beta$ -CD already favored the formation of multiply twinned particles evolving in both icosahedra and nanorods (56%). Under this same reduction kinetics, single-twinned particles evolving into bipyramids were also detected in a low proportion. However, at this  $\beta$ -CD concentration, the concomitant formation of 2D nanoobjects (triangular or disk-like nanoplates) (38%) resulting from a strong kinetic growth regime cannot be avoided.

Increasing the  $\beta$ -CD concentration to a  $\beta$ -CD/Ag molar ratio of 80 led to an almost similar proportion of particles formed from multiply twinned seeds (58%) but with a much higher proportion of icosahedra compared to nanorods evolving from decahedral seeds.<sup>68</sup> This lower proportion of nanorods is expected since a slower growth regime will hinder the formation of the high energy  $\{100\}$  facets compared to the much bigger stabilization effect resulting from a complete coverage by  $\{111\}$  facets as expected for icosahedral particles. Similarly, single-twinned seeds producing bipyramids are not observed anymore since exposing both  $\{100\}$  and  $\{111\}$  facets.<sup>69</sup> The slower growth regime at  $\beta$ -CD/Ag = 80 also led to the almost complete disappearance of the strongly “kinetic” 2D nanoobjects and to the formation of cubic particles resulting from the evolution of single-crystal seeds formed under a slightly slower growth regime than for nanoplates.

At the high  $\beta$ -CD/Ag molar ratio of 150, the even slower retardation effect of  $\beta$ -CD on the growth regime selectively favors the formation of icosahedral particles with a minor proportion of 5-fold-twinned nanorods. Similarly, this even slower growth regime hinders the formation of single crystalline seeds leading to the almost disappearance of cubic particles. Finally, it should be underlined that the initial capping of the seeds by citrate would also block any oxidative etching of the twin defects helping to maintain a high yield of icosahedral particles.<sup>70</sup>

Another point to be considered is the fact that seeds are initially capped by citrate ligands in the “seed solution” and not directly by the  $\beta$ -CD molecules which are only present in the “growth solution”. This suggests that the initial citrate-capped seeds ( $\sim 3$  nm in diameter) can still evolve after their injection into the growth solution. This is in agreement with previous studies showing that Ag seeds are not locked in a final crystalline structure up to  $\sim 10$  nm in diameter.<sup>65</sup> Therefore, a kinetic exchange between citrate and  $\beta$ -CD at the surface of the Ag NPs must also be considered during the initial step of the particle growth. This kinetic exchange will certainly depend on the relative concentrations of  $\beta$ -cyclodextrin and citrate ions.

### 3.2. Formation of Shape-Controlled Pd Nanoparticles.

The interaction of  $\beta$ -CD with palladium differs from the one observed for silver in spite of similar experimental conditions. Instead of forming well-defined faceted NPs, using  $\beta$ -CD to synthesize shape-controlled Pd NPs led to the selective formation of so-called nanodendritic urchin-like particles (Figures 5 and S2, Supporting Information).

This kind of nanostructured morphology was already obtained for Pt,<sup>37,71,72</sup> Au,<sup>73,74</sup> and recently Pd nanoparticles.<sup>75</sup> In the case of Pt, Mahmoud et al.<sup>37</sup> and Wang et al.<sup>71</sup> used PVP as the capping agent in aqueous solution using either tetrahedral platinum nanocrystals seeds<sup>37</sup> or a seedless approach in the presence of formic acid.<sup>71</sup> Lin et al.<sup>72</sup> employed a more complicated procedure using sodium dodecyl sulfate (SDS) and Te nanowires to induce the reduction of  $\text{PtCl}_6^{2-}$  ions via galvanic



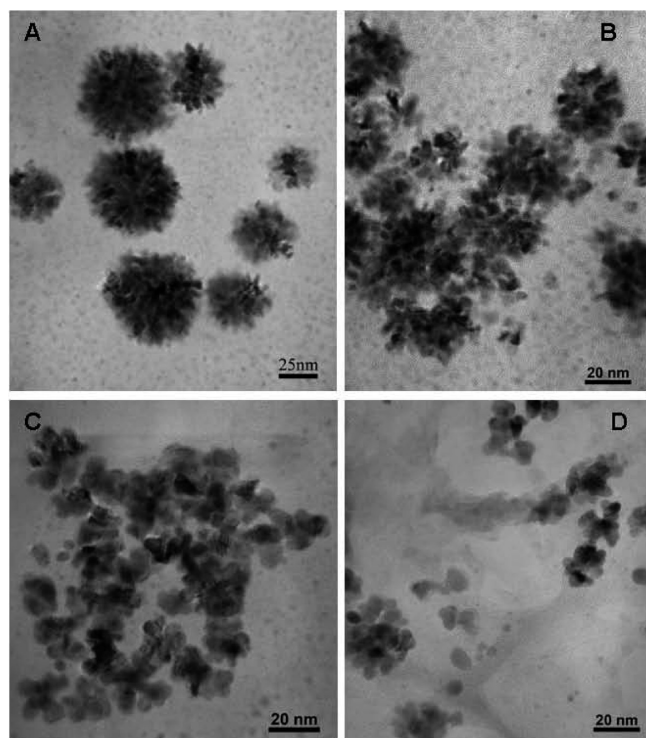


**Figure 5.** TEM images of the Pd nanocrystals obtained at  $\beta$ -CD/Pd molar ratio of (A) 20, (B) 50, (C) 100, and (D) 150.

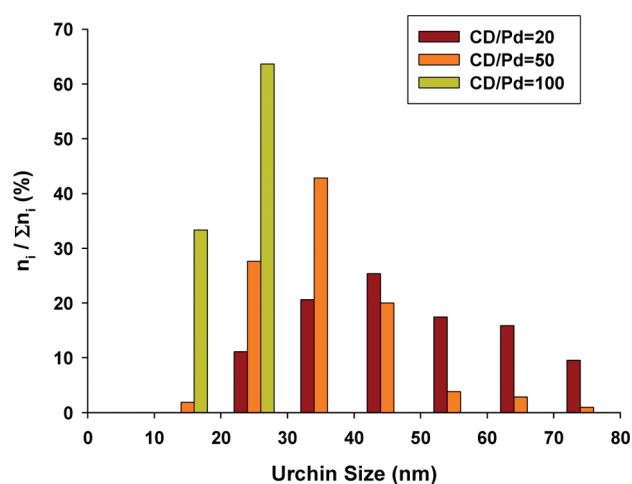


**Figure 6.** Size distributions of the Pd nanodendrites obtained at  $\beta$ -CD/Pd molar ratios of 20, 50, and 100.

replacement. In the case of Au, Bakr et al.<sup>73</sup> used an aqueous approach based on the addition of thiol-terminated carboxylic acids as ligands. Only Lu et al.<sup>74</sup> developed an environmentally friendly method based on the addition of gelatin and silver seeds to a  $\text{HAuCl}_4/\text{K}_2\text{CO}_3$  aqueous solution. For palladium, Lee et al.<sup>75</sup> obtained Pd nanodendrites through the reduction of  $\text{K}_2\text{PdCl}_4$  by ascorbic acid before capping the as-formed NPs by CTAB. However, to our knowledge, nanoparticles with a defined nanodendritic urchin-like morphology were not synthesized up to now, using a “greener” approach.

First of all,  $\beta$ -CD was found necessary to obtain well-defined Pd morphologies. Synthesis performed without the addition of

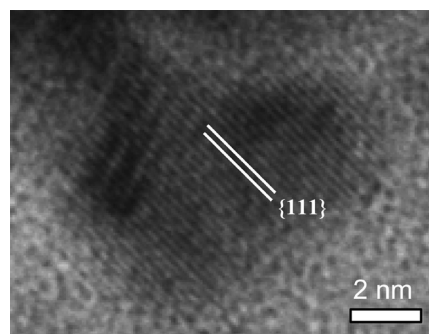


**Figure 7.** HRTEM image showing  $\{111\}$  fringes along a branch of a Pd nanodendrite.

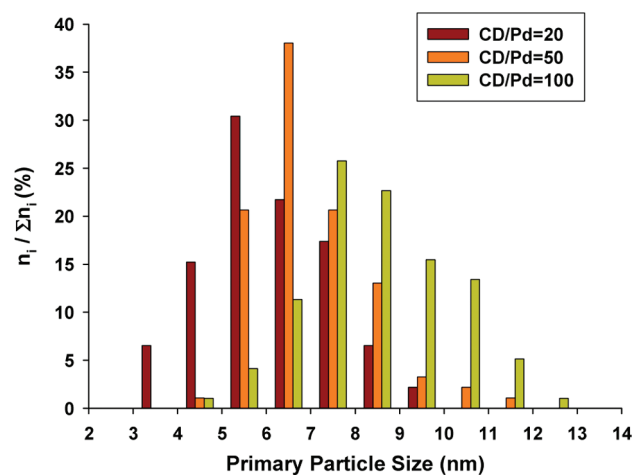


**Figure 8.** Size distributions of the primary particles constituting Pd nanodendrites or Pd multipods at  $\beta$ -CD/Pd molar ratios of 20, 50, and 100.

$\beta$ -CD led only to the formation of spherical Pd NPs presenting a broad size distribution (Figure S3, Supporting Information). At a  $\beta$ -CD/Pd molar ratio of 20, urchin-like particles formed of aggregated primary nanoparticles of  $6.2 \pm 1.3$  nm were selectively obtained. The size of these urchin-like particles is  $47.7 \pm 12.1$  nm showing a relatively broad size distribution (Figure 6). Isolated primary nanoparticles could not be observed on TEM pictures (Figure 5a). HRTEM pictures focused on a branch of an urchin-like particle showed distinct fringes corresponding to a  $d$  spacing of 2.3 Å close to the expected  $d_{111}$  value of 2.25 Å for fcc Pd (Figure 7).

Increasing the  $\beta$ -CD/Pd molar ratio to 50 still results in the formation of nanodendritic particles (Figure 5b). However, their shape looks more irregular suggesting an incomplete and less organized aggregation of the primary particles forming the nanodendritic assemblies. This is confirmed by the presence of some isolated primary NPs that are probably too stabilized by the  $\beta$ -CD molecule to assemble in nanodendrites. This increase in the  $\beta$ -CD concentration also led to a decrease in the particle size to  $35.4 \pm 7.3$  nm (Figure 6). However, the primary NPs aggregated to form urchin-like structures tend to increase slightly in size up to  $6.9 \pm 1.0$  nm (Figure 8). The further increase in the  $\beta$ -CD concentration to reach a  $\beta$ -CD/Pd molar ratio of 100 led to the transformation of the nanostructured particles into multipods formed of 4 to 5 branches (Figure 5c). The formation of

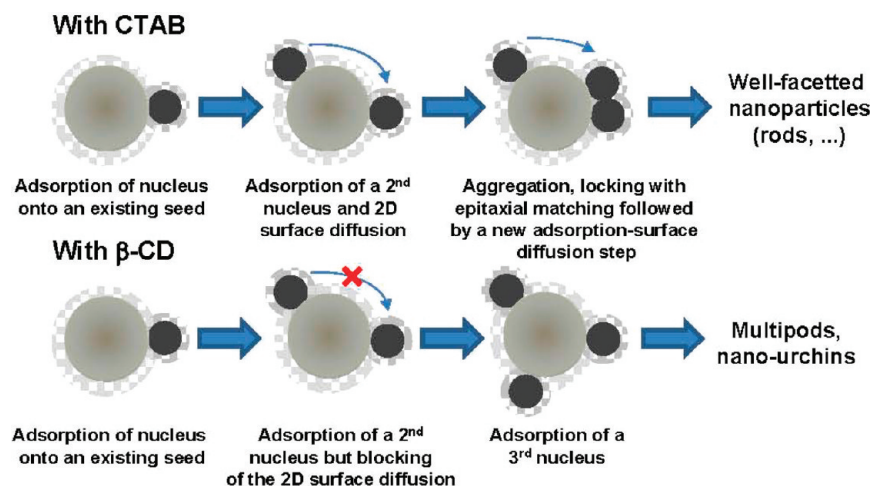


**Figure 9.** Schematic representations of the seed-nuclei attachment process of Pd nanoparticles in the presence of CTAB (top) or  $\beta$ -CD (bottom). Adapted with permission from ref 64.

these multipod particles instead of urchin-like ones obtained at lower  $\beta$ -CD concentration suggests that  $\beta$ -CD restrained the agglomeration of the primary NPs into bigger nanostructured assemblies. The size of the multipods still decreases with increasing concentration of  $\beta$ -CD reaching a value of  $20.9 \pm 2.8$  nm but with a narrower size distribution (Figure 6). On the opposite, the primary NPs assembled into multipods are bigger than those obtained at a  $\beta$ -CD/Pd molar ratio of 20 or 50 ( $10.1 \pm 1.2$  nm) suggesting that once again a higher concentration of  $\beta$ -CD tends to stabilize some of the initial Pd seeds resulting in a lower proportion of seeds able to participate in the formation of the primary NPs (Figure 8). The resulting lower [Pd seed]/[Pd growth] ratio favors the formation of bigger primary particles. Finally, increasing the  $\beta$ -CD concentration to a  $\beta$ -CD/Pd molar ratio of 150 led mainly to isolated NPs and in minor extent to ill-defined multipods.

The use of  $\beta$ -cyclodextrin to form nanostructured Pd particles led to very different morphologies compared to those previously obtained for Ag. Instead of obtaining well-faceted NPs, the interaction of  $\beta$ -CD with Pd led to the formation of nanostructured Pd particles formed of aggregated primary NPs.  $\beta$ -CD regulates the final morphology of these NPs by restraining their final agglomeration leading successively to isolated NPs, multipods, and finally urchin-like particles with decreasing concentration of  $\beta$ -CD. The different interaction strength of  $\beta$ -CD with Pd or Ag could result from the intrinsic structure of the  $\beta$ -CD molecule. Due to the small diameter of the internal cavities of  $\beta$ -CD (up to 0.78 nm), the interaction probably results from hydrophobic–hydrophobic interactions with the Pd nanoparticles as already suggested for Ag,<sup>58</sup> Pt,<sup>60</sup> and Au<sup>76</sup> nanoparticles. This kind of hydrophobic interaction was also observed for Pd nanoparticles but using perthiolated CD molecules.<sup>59</sup> However, since a hydrophobic–hydrophobic interaction is also expected for Ag, such an explanation is not sufficient to describe the formation of nanodendrites or multipods for the particular case of Pd.

In fact, the further organization of these primary NPs into nanodendrites or multipod assemblies might be explained considering recent studies on the formation of Pd nanostructures through seed-mediated synthesis using cetyltrimethylammonium bromide (CTAB) as a directing agent.<sup>53</sup> In this particular

case, it was recently demonstrated that the initial growth of well-faceted Pd NPs predominantly results from an oriented aggregation mechanism of primary NPs therefore differing from the classical crystallization model. In the initial growth stage (in the presence of CTAB), following a second heterogeneous nucleation induced by the injection of seeds into the growth solution, the as-formed primary nuclei tend to aggregate to the growing seeds by sharing the CTAB bilayer (Figure 9). These adsorbed nuclei can then 2D diffuse on the surface of the seeds to reach a more stable configuration which would depend mainly on the size and nature of the seeds. The adsorbed nuclei are then locked onto the seeds through resorption of the CTAB bilayer and epitaxial matching. In such a mechanism as described before, the initial size and structure of the seed would undoubtedly direct the final morphology of the nanocrystal. This initial oriented-attachment mechanism can be followed by molecular reduction when palladium concentration is too low to induce nucleation of secondary particles. In the case of  $\beta$ -CD instead of CTAB, the formation of multipods or dendritic NPs suggests that primary NPs were effectively aggregated to an initial seed. However, the further steps of the accommodation of primary nuclei onto growing seeds (2D surface diffusion to more stable configurations, locking through epitaxial matching and final shape refocusing) seem difficult in the presence of this oligosaccharide molecule. In this respect, the strong hydrophobic interaction of  $\beta$ -CD with Pd would partly block the 2D surface diffusion leading more to an assembly of aggregated NPs than to an ordered oriented growth. Such an effect was not expected for CTAB which is known to act as a poor capping agent.<sup>31</sup> HRTEM observation of multipods and dendritic NPs tends to confirm this hypothesis. Figure 10 shows the HRTEM image of a Pd multipod formed of four different branches. The observation of the  $\{111\}$  fringes showed that epitaxial matching has already occurred on this nanostructured NP leading to the formation of a single crystalline structure. Moreover, three of the four interstitial regions between the four branches locked on the Pd core are disposed at about  $70^\circ$  from each other as expected for primary Pd NPs reorienting themselves to align their  $\{111\}$  facets. This would suggest that epitaxial matching occurs without any particular 2D surface diffusion of these primary NPs on their common Pd core. This also suggests that the interaction of  $\beta$ -CD with



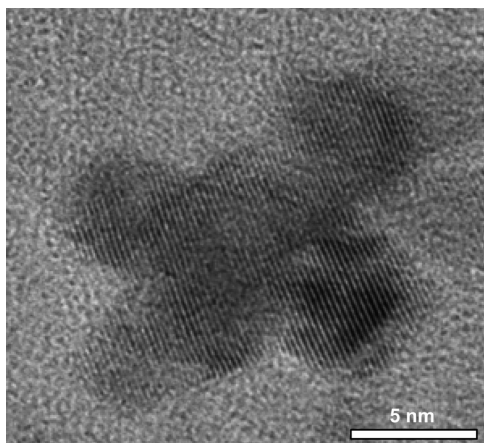


**Figure 10.** HRTEM image of a Pd multipod showing alignment of {111} fringes all along the nanocrystal. The four different branches are disposed around a common Pd core.

palladium is particularly strong. This situation would then differ from the silver case for which a weaker interaction will allow 2D surface diffusion and therefore shape refocusing.

This absence of (or restrained) surface diffusion can also be observed Figure S4 (Supporting Information) showing on a bigger multipod assembly two primary NPs which aligned with the initial Pd core without epitaxial matching. If multipods are generally single crystalline through epitaxial matching of their constituting primary NPs, urchin-like particles formed of a bigger assembly of primary NPs are rarely single crystalline. They generally present large regions on which epitaxial matching already occurred, while other zones are formed of NPs attached in a disordered way to the dendritic assembly (Figure S5, Supporting Information). This would suggest that the epitaxial matching is partly hampered by the  $\beta$ -CD molecule limiting the reorientation of primary NPs in bigger nanoobjects.

Finally, it should be underlined that all the primary NPs are free of twin defects showing a perfect single crystalline nature. This would be surprising if  $\beta$ -CD strongly stabilizes Pd nuclei. However, one possible reason for such an observation might be related to a rapid exchange between citrate and  $\beta$ -CD on the surface of the growing seeds. This rapid exchange would remove the citrate ligand known to protect the initial growing seeds from oxidative etching leading to the consumption of the twin defects and stabilizing seeds as single crystalline nuclei. This also suggests that the interaction of  $\beta$ -CD with Pd is stronger than with Ag for which twinned particles are mainly formed. This lower interaction would then be favorable for the formation of well-faceted NPs.

**3.3. Evaluation of Catalytic Properties of Nanostructured Pd Particles.** After deposition onto  $\text{TiO}_2$ , the as-formed Pd nanodendrites or multipods were subsequently evaluated for the hydrogenation of an  $\alpha,\beta$  unsaturated aldehyde, i.e., cinnamaldehyde. The reaction scheme of the cinnamaldehyde hydrogenation occurs in our case via parallel and consecutive pathways that involve hydrogenation of  $\text{C}=\text{O}$  and  $\text{C}=\text{C}$  groups forming cinnamyl alcohol (CA), hydrocinnamaldehyde (HCALD), and 3-phenylpropanol (PP). On Pd catalytic systems, the reaction occurs preferentially through the initial hydrogenation of the  $\text{C}=\text{C}$  bond leading to hydrocinnamaldehyde, whereas selective  $\text{C}=\text{O}$  bond hydrogenation is limited.<sup>77</sup> The reaction scheme herein is formed of two parallel pathways, one corresponding

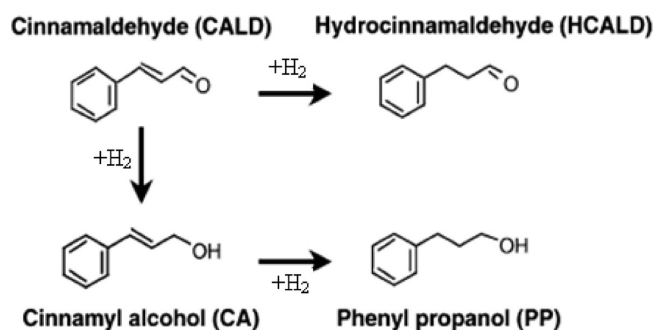


**Figure 11.** Reaction scheme in the hydrogenation of cinnamaldehyde over Pd/TiO<sub>2</sub> catalysts.

**Table 3.** Pd Contents, Initial Rate Constants, Selectivity Results (at 20% Conversion), and TOF Values of the Nanostructured Pd(*x*)/TiO<sub>2</sub> Catalysts with *x* =  $\beta$ -CD/Pd Molar Ratio<sup>a</sup>

catalyst	Pd content (wt%)	initial rate constant ( $10^{-6}$ mol $\text{g}^{-1}$ $\text{s}^{-1}$ )	TOF ( $\text{s}^{-1}$ )	selectivity (%)		
				HCALD	PP	CA
Pd(20)/TiO <sub>2</sub>	0.21	6.0	1.7	49	50	1
Pd(50)/TiO <sub>2</sub>	0.19	6.1	2.1	51	47	2
Pd(100)/TiO <sub>2</sub>	0.20	3.8	1.8	49	50	1
Pd/TiO <sub>2</sub> ref.	0.40	11.9	1.4	46	51	3

<sup>a</sup> HCALD, PP, and CA refer, respectively, to the following products: hydrocinnamaldehyde, 3-phenyl-1-propanol, and cinnamyl alcohol. Comparison is provided to a Pd/TiO<sub>2</sub> reference prepared by simple impregnation without using  $\beta$ -CD.

to a preferential  $\text{C}=\text{C}$  bond hydrogenation of cinnamaldehyde into hydrocinnamaldehyde and another one leading through the initial hydrogenation of the  $\text{C}=\text{O}$  bond to cinnamyl alcohol followed by the rapid hydrogenation into 3-phenyl-1-propanol (Figure 11).

Initial rate constants are reported in Table 3 for the different Pd/TiO<sub>2</sub> catalysts prepared at  $\beta$ -CD/Pd molar ratios of 20, 50, and 100. Comparison was also provided with an isotropic Pd/TiO<sub>2</sub> reference catalyst prepared in the absence of  $\beta$ -CD by simple impregnation. Similar values are observed for the Pd(20)/TiO<sub>2</sub> and Pd(50)/TiO<sub>2</sub> catalysts, while the initial rate constant decreased for Pd(100)/TiO<sub>2</sub>. This lower rate constant is expected if the size of the primary particles forming nanodendritic or multipod Pd particles is taken into account. While relatively similar Pd sizes were found at  $\beta$ -CD/Pd ratios of 20 and 50 (6.2–6.9 nm), bigger Pd sizes were obtained at the  $\beta$ -CD/Pd ratio of 100 (10.1 nm). This bigger particle size leads to a lower surface-to-volume ratio and therefore to a lower number of surface Pd sites available for reaction in the case of Pd(100)/TiO<sub>2</sub>. Similarly, on the Pd/TiO<sub>2</sub> reference, the initial rate constant reaches a higher value due to its higher Pd loading (0.4 wt %) for similar Pd particle size (5.6 nm).

Determination of turnover frequency values (TOF) for each catalyst provides information about the intrinsic catalytic activity per surface Pd site. TOF values were determined taking into account the size of the primary particles forming each bigger

assembly and considering a fcc cubooctahedral model according to Van Hardeveld and Hartog.<sup>78</sup> It should however be kept in mind that this rough approximation would lead to an overestimation of the surface Pd sites available for reaction (and then an underestimation of TOF values). These TOF values are reported in Table 3. For all the catalysts, relatively similar values were found going from 1.7 to 2.1 s<sup>-1</sup> showing that the intrinsic catalytic activity per surface Pd site is not modified by the various amounts of  $\beta$ -cyclodextrin used for their preparation. These TOF values are slightly higher than on the Pd/TiO<sub>2</sub> reference. It therefore confirms that the lower intrinsic rate observed for Pd(100)/TiO<sub>2</sub> was only due to a lower surface-to-volume ratio. It should be noted that the turnover values obtained are similar to Pd systems evaluated at similar temperature and pressure conditions and supported on Al<sub>2</sub>O<sub>3</sub> (TOF = 2.7 s<sup>-1</sup>),<sup>79</sup> activated carbon (2.7–4.1 s<sup>-1</sup>),<sup>80</sup> or titanate nanotubes (1.1 s<sup>-1</sup>) showing that the presence of  $\beta$ -CD at the surface of the Pd particles apparently does not interfere negatively on the catalytic properties of the final nanostructured catalysts.

Selectivity results were also similar whatever the Pd/TiO<sub>2</sub> catalyst (Table 3). At a 20% conversion level, selectivities to hydrocinnamaldehyde (HCALD) and to 3-phenyl-1-propanol (PP) are both close to 50%, while only a residual amount of cinnamyl alcohol (CA) was found. This low selectivity is characteristic of Pd catalysts.<sup>82</sup> The selectivity to HCALD is also lower than generally obtained for supported Pd catalytic systems.<sup>79,81</sup> For the hydrogenation of cinnamaldehyde, selectivity changes are known to depend on the type of crystallographic planes exposed,<sup>83</sup> the size of the metallic particles, and support effects.<sup>77</sup> In the present case, the size does not seem to play a significant role since increasing the size of the primary particles from 6.2 to 10.1 nm (from Pd(20)/TiO<sub>2</sub> to Pd(100)/TiO<sub>2</sub>) did not change the selectivity results. The same conclusion can be reached considering the Pd/TiO<sub>2</sub> reference catalyst. TEM characterizations have otherwise shown that primary particles are mainly composed of (111) planes, while selectivity to HCALD is about 50% on each catalyst. This observation is in agreement with the theoretical study of Delbecq et al.<sup>83</sup> who found that the (111) orientation of palladium favors simultaneous adsorption on the C=C and C=O bonds of the cinnamaldehyde molecule leading to the formation of HCALD and CA, the latter being rapidly hydrogenated into PP. This relative good agreement between predictions on selectivity results based on crystallographic planes exposed and experimental results also suggests that electronic modifications induced by the support are minimal in the present case due to the weakly interacting nature of the low surface area TiO<sub>2</sub> support used herein.

#### 4. CONCLUSION

$\beta$ -Cyclodextrin was used successfully for the first time to synthesize shape-controlled Ag and Pd nanoparticles using a seeding-mediated technique with initially citrate-capped seeds. While  $\beta$ -CD mainly led to the synthesis of well-faceted icosahedra, silver, multipods, or nanodendrites made by the assembly of primary nanoparticles were observed for palladium. This different behavior of  $\beta$ -CD with palladium compared to silver may result from a different interaction affinity of  $\beta$ -CD with these two metals. In the case of silver, the role of  $\beta$ -CD would be to regulate the size of the growing seeds to stabilize seeds in a given structure (multiply or single-twinned, single crystalline) controlling the final nanocrystal morphology. In the case of palladium, the

stabilization effect induced by the oligosaccharide molecule would restrict the formation of nanostructured particles to morphologies resulting from the aggregation of primary nanoparticles. Finally, after deposition onto TiO<sub>2</sub>, Pd particles were found to be intrinsically active in the hydrogenation of cinnamaldehyde. Further studies will be centered on a comprehensive analysis of the  $\beta$ -CD interaction with the surface of Pd or Ag nanoparticles.

#### ■ ASSOCIATED CONTENT

**S Supporting Information.** TEM images of different Ag or Pd nanostructures obtained using  $\beta$ -CD and of spherical Pd particles obtained without using  $\beta$ -CD. HRTEM images of Pd multipod and of a Pd nanodendrite at the early stage of formation. This material is available free of charge via the Internet at <http://pubs.acs.org>.

#### ■ AUTHOR INFORMATION

##### Corresponding Author

\*Phone: +33-472-44-53-20. Fax: +33-472-44-53-99. E-mail: [gilles.berhault@ircelyon.univ-lyon1.fr](mailto:gilles.berhault@ircelyon.univ-lyon1.fr). Phone: +216-79-325-250. Fax: +216-79-325-314. E-mail: [h\\_kochkar@yahoo.fr](mailto:h_kochkar@yahoo.fr).

#### ■ ACKNOWLEDGMENT

This work has been supported by the “Action Intégrée Franco-Tunisienne du Ministère des Affaires Étrangères et Européennes Français et du Ministère de l'Enseignement Supérieur de la Recherche Scientifique et de la Technologie Tunisien”.

#### ■ REFERENCES

- (1) El-Sayed, M. A. *Acc. Chem. Res.* **2001**, *34*, 257.
- (2) Murphy, C. J.; Sau, T. K.; Gole, A. M.; Orendorff, C. J.; Gao, J.; Gou, L.; Hunyadi, S. E.; Li, T. *J. Phys. Chem. B* **2005**, *109*, 13857.
- (3) Kumar, P. S.; Pastoriza-Santos, I.; Rodríguez-González, B.; García de Abajo, F. J.; Liz-Marzán, L. M. *Nanotechnology* **2008**, *19*, 015606.
- (4) Hao, E.; Schatz, G. C.; Hupp, J. T. *J. Fluoresc.* **2004**, *14*, 331.
- (5) Lee, K. S.; El-Sayed, M. A. *J. Phys. Chem. B* **2006**, *110*, 19220.
- (6) Perez-Juste, J.; Pastoriza-Santos, I.; Liz-Marzán, L. M.; Mulvaney, P. *Coord. Chem. Rev.* **2005**, *249*, 1870.
- (7) Nikoobakht, B.; Wang, Z.; El-Sayed, M. A. *Chem. Phys. Lett.* **2002**, *366*, 17.
- (8) Sudeep, P. K.; Shibu, J. S. T.; George, T. K. *J. Am. Chem. Soc.* **2005**, *127*, 6516.
- (9) Telkar, M. M.; Rode, C. V.; Chaudhari, R. V.; Joshi, S. S.; Nalawade, A. M. *Appl. Catal., A* **2004**, *273*, 11.
- (10) Miyazaki, A.; Balint, I.; Aika, K. *Phys. Chem. Chem. Phys.* **2004**, *6*, 2000.
- (11) Chimentao, R. J.; Kirm, I.; Medina, F.; Rodriguez, X.; Cesteros, Y.; Salagre, P.; Sueiras, J. E. *Chem. Commun.* **2004**, 846.
- (12) Narayanan, R.; El-Sayed, M. A. *Nano Lett.* **2004**, *4*, 1343.
- (13) Berhault, G.; Bisson, L.; Thomazeau, C.; Verdon, C.; Uzio, D. *Appl. Catal., A* **2007**, *327*, 32.
- (14) Bratlje, K. M.; Lee, H.; Komvopoulos, K.; Yang, P.; Somorjai, G. A. *Nano Lett.* **2007**, *7*, 3097.
- (15) Wang, C.; Daimon, H.; Lee, Y.; Kim, J.; Sun, S. *J. Am. Chem. Soc.* **2007**, *129*, 6974.
- (16) Hernandez, J.; Solla-Gullon, J.; Herrero, E.; Aldaz, A.; Feliu, J. M. *J. Phys. Chem. C* **2007**, *111*, 14078.
- (17) Piccolo, L.; Valcarcel, A.; Bausach, M.; Thomazeau, C.; Uzio, D.; Berhault, G. *Phys. Chem. Chem. Phys.* **2008**, *10*, 5504.
- (18) Christopher, P.; Linic, S. *J. Am. Chem. Soc.* **2008**, *130*, 11264.

- (19) Lee, I.; Delbecq, F.; Morales, R.; Albitzer, M. A.; Zaera, F. *Nat. Mater.* **2009**, *8*, 132.
- (20) Tsung, C. K.; Kuhn, J. N.; Huang, W.; Aliaga, C.; Hung, L. I.; Somorjai, G. A.; Yang, P. J. *Am. Chem. Soc.* **2009**, *131*, 5816.
- (21) Sun, Y.; Xia, Y. *Science* **2002**, *298*, 2176.
- (22) Murphy, C. J.; Jana, N. *Adv. Mater.* **2002**, *14*, 80.
- (23) Seo, D.; Park, J. C.; Song, H. *J. Am. Chem. Soc.* **2006**, *128*, 14863.
- (24) Lim, B.; Xiong, Y.; Xia, Y. *Angew. Chem., Int. Ed.* **2007**, *46*, 9279.
- (25) Li, C.; Shuford, K. L.; Park, Q. H.; Cai, W.; Li, Y.; Lee, E. J.; Cho, S. O. *Angew. Chem., Int. Ed.* **2007**, *46*, 3264.
- (26) Heo, J.; Kim, D. S.; Kim, Z. H.; Lee, Y. W.; Kim, D.; Kim, M.; Kwon, K.; Park, H. J.; Yun, W. S.; Han, S. W. *Chem. Commun.* **2008**, 6120.
- (27) Chang, C. C.; Wu, H. L.; Kuo, C. H.; Huang, M. H. *Chem. Mater.* **2008**, *20*, 7570.
- (28) Niu, W.; Zeng, S.; Wang, D.; Liu, X.; Li, H.; Han, S.; Chen, J.; Tang, Z.; Xu, G. *J. Am. Chem. Soc.* **2009**, *131*, 697.
- (29) Seo, D.; Yoo, C. I.; Chung, I. S.; Park, S. M.; Ryu, S.; Song, H. *J. Phys. Chem. C* **2008**, *112*, 2469.
- (30) Xu, J.; Li, S.; Weng, J.; Wang, X.; Zhou, Z.; Yang, K.; Liu, M.; Chen, X.; Cui, Q.; Cao, M.; Zhang, Q. *Adv. Funct. Mater.* **2008**, *18*, 277.
- (31) Berhault, G.; Bausach, M.; Bisson, L.; Becerra, L.; Thomazeau, C.; Uzio, D. *J. Phys. Chem. C* **2007**, *111*, 5915.
- (32) Zhang, Q.; Xie, J.; Yang, J.; Lee, J. Y. *ACS Nano* **2009**, *3*, 139.
- (33) Kim, D.; Heo, J.; Kim, M.; Lee, Y. W.; Han, S. W. *Chem. Phys. Lett.* **2009**, *468*, 245.
- (34) Kou, X.; Ni, W.; Tsung, C. K.; Chan, K.; Lin, H. Q.; Stucky, G. D.; Wang, J. *Small* **2007**, *3*, 2103.
- (35) Wiley, B. J.; Xiong, Y.; Li, Z. Y.; Yin, Y.; Xia, Y. *Nano Lett.* **2006**, *6*, 765.
- (36) Zettsu, Z.; McLellan, J. M.; Wiley, B.; Yin, Y.; Li, Z. Y.; Xia, Y. *Angew. Chem., Int. Ed.* **2006**, *45*, 1288.
- (37) Mahmoud, M. A.; Tabor, C. E.; El-Sayed, M. A.; Ding, Y.; Wang, Z. L. *J. Am. Chem. Soc.* **2008**, *130*, 4590.
- (38) Watt, J.; Young, N.; Haigh, S.; Kirkland, A.; Tilley, R. D. *Adv. Mater.* **2009**, *21*, 2288.
- (39) Umar, A. A.; Oyama, M. *Cryst. Growth Des.* **2009**, *9*, 1146.
- (40) Wiley, B.; Sun, Y.; Mayers, B.; Xia, Y. *Chem.—Eur. J.* **2005**, *11*, 454.
- (41) Lofton, C.; Sigmund, W. *Adv. Funct. Mater.* **2005**, *15*, 1197.
- (42) Wiley, B.; Herricks, T.; Sun, Y.; Xia, Y. *Nano Lett.* **2004**, *4*, 1733.
- (43) Gole, A.; Murphy, C. J. *Chem. Mater.* **2004**, *16*, 3633.
- (44) Sau, T. K.; Murphy, C. J. *Langmuir* **2004**, *20*, 6414.
- (45) Xiong, Y.; Chen, J.; Wiley, B.; Xia, Y.; Yin, Y.; Li, Z. Y. *Nano Lett.* **2005**, *5*, 1237.
- (46) Pérez-Juste, J.; Liz-Marzán, L. M.; Carnie, S.; Chan, D. Y. C.; Mulvaney, P. *Adv. Funct. Mater.* **2004**, *14*, 571.
- (47) Iqbal, M.; Chung, Y. L.; Tae, G. *J. Mater. Chem.* **2007**, *17*, 335.
- (48) Gao, J.; Bender, C. M.; Murphy, C. J. *Langmuir* **2003**, *19*, 9065.
- (49) Kou, X.; Zhang, S.; Tsung, C. K.; Yeung, M. H.; Shi, Q.; Stucky, G. D.; Sun, L.; Wang, J.; Yan, C. *J. Phys. Chem. B* **2006**, *110*, 16377.
- (50) Kou, X.; Zhang, S.; Tsung, C. K.; Yang, Z.; Yeung, M. H.; Stucky, G. D.; Sun, L.; Wang, J.; Yan, C. *Chem.—Eur. J.* **2007**, *13*, 2929.
- (51) Gou, L.; Murphy, C. J. *Chem. Mater.* **2005**, *17*, 3668.
- (52) Cheong, S.; Watt, J.; Ingham, B.; Toney, M. F.; Tilley, R. D. *J. Am. Chem. Soc.* **2009**, *131*, 14590.
- (53) Bisson, L.; Boissière, C.; Nicole, L.; Grosso, D.; Jolivet, J. P.; Thomazeau, C.; Uzio, D.; Berhault, G.; Sanchez, C. *Chem. Mater.* **2009**, *21*, 2668.
- (54) Huang, Y.; Li, D.; Li, J. *Chem. Phys. Lett.* **2004**, *389*, 14.
- (55) Huang, T.; Meng, F.; Qi, L. *J. Phys. Chem. C* **2009**, *113*, 13636.
- (56) Dickson, J.; Geckeler, K. E. *Langmuir* **2009**, *25*, 13224.
- (57) Huang, T.; Meng, F.; Qi, L. *Langmuir* **2010**, *26*, 7582.
- (58) Ng, C. H. B.; Yang, J.; Fan, W. Y. *J. Phys. Chem. C* **2008**, *112*, 4141.
- (59) Alvarez, J.; Liu, J.; Roman, E.; Kaifer, A. E. *Chem. Commun.* **2000**, 1151.
- (60) Giuffrida, S.; Ventimiglia, G.; Petralia, S.; Conoci, S.; Sortino, S. *Inorg. Chem.* **2006**, *45*, 508.
- (61) Szejli, J. *Chem. Rev.* **1998**, *98*, 1743.
- (62) Jana, N.; Gearheart, L.; Murphy, C. J. *J. Phys. Chem. B* **2001**, *105*, 4065.
- (63) Johnson, C. J.; Dujardin, E.; Davis, S. A.; Murphy, C. J.; Mann, S. *J. Mater. Chem.* **2002**, *12*, 1765.
- (64) Yin, Y.; Alivisatos, A. P. *Nature* **2005**, *437*, 664.
- (65) Xiong, Y.; Xia, Y. *Adv. Mater.* **2007**, *19*, 3385.
- (66) Ajayan, P. M.; Marks, L. D. *Phys. Rev. Lett.* **1998**, *80*, 585.
- (67) Cleveland, C.; Landman, U. *J. Chem. Phys.* **1991**, *94*, 7376.
- (68) Pietrobon, B.; McEachran, M.; Kitaev, V. *ACS Nano* **2009**, *3*, 21.
- (69) Benlekber, S.; Epicier, T.; Bausach, M.; Aouine, M.; Berhault, G. *Philos. Mag. Lett.* **2009**, *89*, 145.
- (70) Xiong, Y.; McLellan, J. M.; Yin, Y.; Xia, Y. *Angew. Chem., Int. Ed.* **2007**, *46*, 790.
- (71) Wang, L.; Guo, S.; Zhai, J.; Dong, S. *J. Phys. Chem. C* **2008**, *112*, 13372.
- (72) Lin, Z. H.; Lin, M. H.; Chang, H. T. *Chem.—Eur. J.* **2009**, *15*, 4656.
- (73) Bakr, O. M.; Wunsch, B. H.; Stellacci, F. *Chem. Mater.* **2006**, *18*, 3297.
- (74) Lu, L.; Ai, K.; Ozaki, Y. *Langmuir* **2008**, *24*, 1058.
- (75) Lee, Y. W.; Kim, M.; Han, S. W. *Chem. Commun.* **2010**, 46, 1535.
- (76) Liu, Y.; Male, K. B.; Bouvrette, P.; Luong, J. H. T. *Chem. Mater.* **2003**, *15*, 4172.
- (77) Gallezot, P.; Richard, D. *Catal. Rev. Sci. Eng.* **1998**, *40*, 81.
- (78) Van Hardeveld, R.; Hartog, F. *Surf. Sci.* **1969**, *15*, 189.
- (79) Lashdaf, M.; Krause, A. O. I.; Lindblad, M.; Tiita, M.; Venäläinen, T. *Appl. Catal. A* **2003**, *241*, 65.
- (80) Cabiach, A.; Cacciaguerra, T.; Trens, P.; Durand, R.; Delahay, G.; Medevielle, A.; Plée, D.; Coq, B. *Appl. Catal. A* **2008**, *340*, 229.
- (81) Jabou, K.; Kochkar, H.; Berhault, G.; Ghorbel, A. *J. Mater. Sci.* **2009**, *44*, 6677.
- (82) Rylander, P. N. *Catalytic Hydrogenation in Organic Synthesis*; Academic Press: New York, 1979; p 72.
- (83) Delbecq, F.; Sautet, P. *J. Catal.* **1995**, *152*, 217.